Long-wavelength mid-infrared reflectors using guided-mode resonance

Kou-Wei Lai, Sheng-Di Lin,* Zong-Lin Li, and Chi-Cheng Wang

Department of Electronics Engineering, National Chiao Tung University, 1001 University Road, Hsinchu 300, Taiwan

*Corresponding author: sdlin@mail.nctu.edu.tw

Received 29 January 2013; revised 22 July 2013; accepted 5 September 2013;
posted 6 September 2013 (Doc. ID 184332); published 26 September 2013

We have proposed and fabricated a new mid-infrared reflector using the guided-mode resonance (GMR). The GMR reflector consists of subwavelength Ge grating on GaAs substrate with a low-refractive-index SiO_x layer in between. With a total thickness of about 2 μm, a near-100% reflectivity at 8 μm has been obtained both theoretically and experimentally. © 2013 Optical Society of America

OCIS codes: (050.2770) Gratings; (230.4040) Mirrors.

http://dx.doi.org/10.1364/AO.52.006906

1. Introduction

Semiconductor-based optoelectronic devices for long-wavelength mid-infrared (IR) regime (8–12 μm) have been studied for decades due to their wide applications in biosensing, thermal imaging, and communication [1,2]. To develop these devices, a high-reflectivity mirror is necessary in certain circumstances. Metal film is commonly used for this purpose. However, because of its broadband (from visible to THz) high reflectivity, it is sometimes inconvenient if one wishes to have a definite reflectivity only in a particular wavelength range. Consisting of alternative layers with high/low refractive indexes, the semiconductor or dielectric distributed-Bragg-reflectors (DBRs) can provide an on-demand bandpass filter with a proper design and selection of materials. Nevertheless, it is not practical to apply them for long-wavelength IR devices, as the total film thickness needed is far too thick, which makes sample growth and device fabrication more difficult.

On the other hand, the emerging subwavelength grating has attracted much attention recently due to its novel optical properties and flexibility in integrating with other devices [3–11]. The pioneering works [3–6] demonstrated that the two-dimensional gratings using the guided-mode resonance (GMR) effect can become a new element in optical devices in visible and near-IR regimes. With a single layer serving as a grating and also a waveguide, the subwavelength grating exhibits wideband high reflectivity. The physical origin of the wideband reflectivity of these high-contrast subwavelength gratings that we shall employ in this work has been discussed in [12,13] for 1D and 2D gratings, respectively. The much thinner thickness and flexibility during device processing enables us to fabricate a high-reflectivity mirror in a desired band in the long-wavelength mid-IR regime. Such a reflector can be used, for example, to fabricate a resonant cavity to enhance the quantum efficiency of the quantum-dot IR photodetectors with responsivity spectra ranging from 7.5 to 8.5 μm [14,15]. These GMR reflectors can find their applications aiming for different wavelengths in mid-IR regime due to their flexibility. In this paper, we propose and demonstrate the use of a GMR reflector as a high-reflectivity mirror at the wavelength of 8 μm. A theoretical simulation, device fabrication, and reflectivity measurement will be presented and discussed. GMR reflectors aiming for longer (>100 μm) [16] and shorter (2–3 μm) [17] wavelengths have been reported previously.

1559-128X/13/286906-04$15.00/0
© 2013 Optical Society of America

2. Structure Design and Implementation

GMR is a coupling effect between the grating diffraction and the waveguide mode [3–7]. The reason for achieving nearly 100% reflectivity is that, as the diffracted rays couple into the guided mode of grating, a resonant condition can be met to make the transmitted light interference destructively. One obvious advantage of using a GMR mirror is its much thinner thickness ($\sim\lambda$, the designed wavelength) compared with that of a DBR reflector ($\sim 10\lambda$). Our proposed structure is sketched schematically in Fig. 1. On a semi-insulating GaAs substrate, an SiO_x layer is followed by a Ge subwavelength grating [see Fig. 1(a)]. We use Ge as the grating material for two reasons. First, the refractive index of Ge is 4.0 at 8 μm, so the total thickness of a Ge thin film can be reduced to less than 1 μm (which we will see from the simulation). This makes the subsequent grating fabrication using a lift-off process much easier. The second reason is the near-100% transparency of Ge at 8 μm. The low-refractive-index SiO_x layer sandwiched by the GaAs substrate and the Ge layer is used to enhance the waveguiding effect in the Ge grating/waveguide.

We perform the numerical simulation based on the method of rigorous coupled-wave analysis [18] that calculates the diffraction of the incident plane waves. By using the commercial software DiffractMOD 3.1 produced by RSoft Design Group, with input structure parameters of thickness and refractive index of each material, the reflectivity spectra and steady-state electric field distribution can be calculated three dimensionally [19]. The refractive indexes of GaAs and Ge are set as 3.4 and 4.0, respectively. SiO_x has a sharp and strong absorption at 10 μm, so we take the dispersion relation (n and k) from the software library. As shown in Fig. 1(b), hexagonal-lattice Ge gratings (period $a = 5$ μm) and circular holes with various radius ($r = 1.55$ – 1.85 μm) are used for simulation. The film thicknesses of SiO_x and Ge are 1.3 and 0.78 μm, respectively. One has to consider the fabrication issue when these parameters are chosen if the standard photolithography process is to be employed. Note that the boundary of the simulated structure has been put far enough and set as perfect matching layers to avoid any boundary effect.

The simulated reflective spectra are plotted in Fig. 2. Let us look at the spectra of r/a ratio (the ratio between the hole radius r and the period a) of 0.31 first (black curve). It is clear that there is a high-reflectivity band from 8 to 10 μm. The abrupt drop at 10 μm results from the strong absorption of SiO_x. The reflectivity higher than 95% in 8–10 μm has been achieved. With an increasing r/a ratio, the high-reflectivity band exhibits a blue shift, which is due to the increased effective refractive index of the Ge waveguide with the higher r/a ratio [8]. Note that the long-wavelength side is limited by the SiO_x absorption at 10 μm.

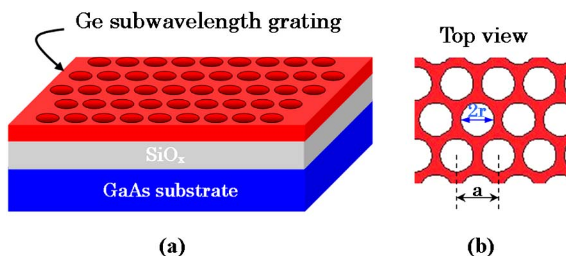

Fig. 1. Schematic structure of the (a) GMR reflector and (b) its top view. The hole radius is r and the center-to-center distance of the holes is a.

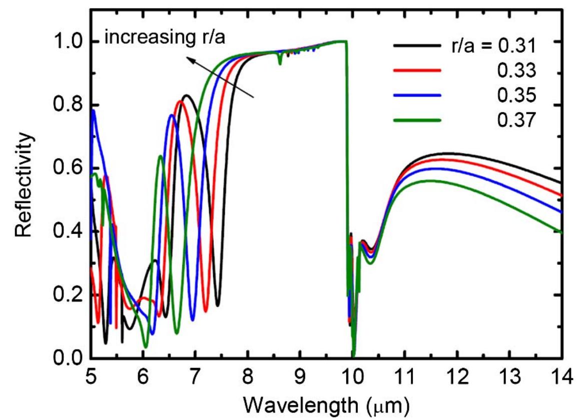

Fig. 2. Simulated reflectivity spectra for various r/a ratios.

To obtain a clear picture of the GMR effect in our structure, we plot the simulated electric field distributions of the device with r/a ratio of 0.35 for three wavelengths (8.00, 6.56, and 6.95 μm) in Fig. 3. Because the device is a 3D structure, we plot the distribution along the axis at the hole center (C), as indicated in the inset of Fig. 3. Note that the rectangle in the inset figure is the unit cell for simulation. The electric distribution along the axis on the sidewall (S) of the unit cell is also plotted for the wavelength of 8 μm. The wavelengths of 8.00 and 6.56 μm are selected because of their high reflectivity and the wavelength of 6.95 μm is the local minimum of reflectivity, as shown by the spectra for the 0.35 r/a ratio in Fig. 2.

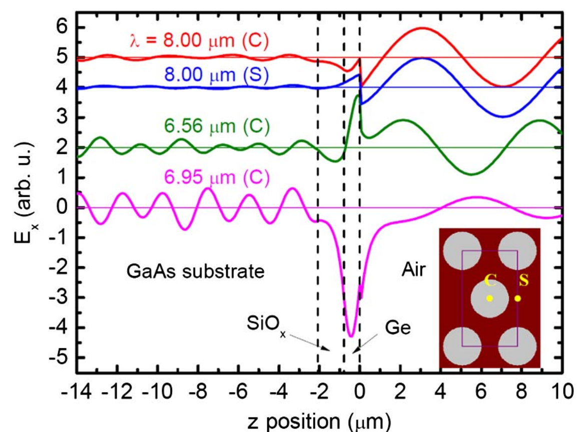

Fig. 3. Simulated electric field distributions for three wavelengths for the device of $r/a = 0.35$. The two distributions along the center (C) and side (S) lines are plotted for 8.00 μm, as indicated by the unit cell in the inset. The spectra are vertically shifted for clarity.

Let us first look at the C-axis electric field distribution of the 8 μm one in Fig. 3 (red curve). It is clear that the field intensity in the air region is much larger than that in the GaAs substrate, indicating its high reflectivity of ~0.96. The similar situation can be seen in the S-axis one. In the case of 6.56 μm at the C axis, the transmitted wave gets stronger but still weaker than the reflected one, so the reflectivity lowers a bit to about 0.78. The last one of 6.95 μm at the C axis exhibits a strong transmission, as its reflectivity is at the local minimum. It is also found that the 6.56 μm one is a higher-order mode because there is a node in the waveguide region.

3. Sample Preparation and Measurement

The sample preparation starts from a (100) GaAs substrate. After cleaning with acetone and de-ionized water, the native oxide on the GaAs wafer is removed by a solution of $\mathrm{HCL:H_2O} = 1:10$. Then, 1.3-μm-thick SiO_x is deposited at 80°C by plasma-enhanced chemical-vapor-deposition (PECVD). With the standard photolithography, the photoresist in the region of holes is formed. In the following, the Ge thin film (thickness = 0.78 μm) is evaporated by an e-gun evaporator at room temperature and then the unwanted Ge is lift-off in acetone. Each device has an area of 5 mm × 5 mm. The photo image of the finished device taken by an optical microscopy is shown in Fig. 4(a). The large area picture shows good uniformity of the fabricated device. The scanning electron microscopy (SEM) image in Fig. 4(b) illustrates that the holes in the hexagonal lattice have nearly perfect circular shape. The diameters of each device are also measured with the SEM pictures.

The spectra measurement is performed in air at room temperature. To avoid the calibration problem of the transmission measurement [20], we measure the reflectivity spectra by combining a commercial Fourier-transformed infrared (FTIR, Nicolet 6700) with a homemade optical setup, as illustrated in Fig. 4(c). The personal computer (PC)-controlled FTIR system includes a light source, a photodetector, and optics for the wavelength range of 2–25 μm. The light source is fixed in the FTIR equipment, and its light is collimated into plane waves by the existing lens before incident onto the sample. The sample attached to the sample holder is placed in the middle between the light source and the built-in IR detector. The 45°-tilted ZnSe 50/50 beam splitter is used to redirect the reflected light from the sample surface to the mirror 1 (M1). With the three reflections on mirrors 1, 2, and 3 (M1, M2, and M3), the reflected light is detected by the IR detector. The spot size of the incident light is about 3 mm × 3 mm, which is defined with a square aperture in front of the sample. By replacing the sample with a gold thin film prepared by an e-gun evaporator, we can calibrate the reflectivity by assuming that the reflectivity of gold in this regime is known as 0.98.

In Fig. 5, we plot the measured reflectivity spectra for four devices with various r/a ratios ranging from 0.330 to 0.370. A high reflectivity at 8 μm is obtained unambiguously. Note that we have prepared and measured several samples for each r/a ratio, and they reveal nearly the same high-reflectivity band. With the increasing r/a ratio (larger holes), the band of high reflectivity shifts to the shorter wavelength, as expected in Fig. 2. However, the reflectivity drops to less than 90% when the wavelength is longer than about 9 μm, which is not consistent with the simulation. We believe that this is caused by the absorption of the PECVD-prepared SiO_x layer. It has been reported that the absorption of an SiO_x layer is strongly dependent on the preparation method [21]. This is also evidenced by the broad reflectivity dip at about 10 μm. The broader dip differing from the theoretical simulation indicates that the SiO_x prepared by PECVD at 80°C has a wider absorption band compared with that used in our simulation. This wide absorption band could have extended to the wavelength of 8.5–9.5 μm and thereby lowered the reflectivity. To confirm this, we also prepare a

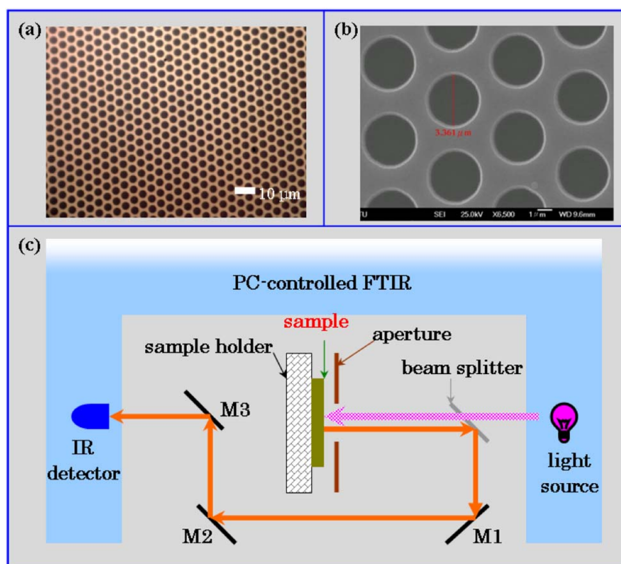

Fig. 4. (a) Optical microscopic and (b) SEM images of one fabricated sample (r/a ratio = 0.33). (c) Schematic setup for reflectivity spectra measurement.

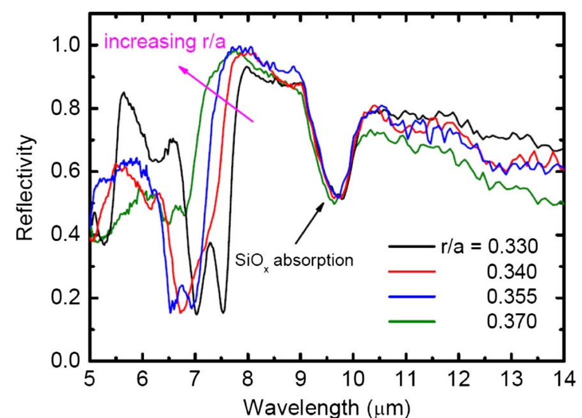

Fig. 5. Measured reflectivity spectra for various r/a ratios.

single-layer SiO_x on GaAs. By measuring and fitting its reflectivity spectra, we can extract its n and k values. The result (not shown here) reveals an increased k value of PECVD-prepared SiO_x between 8 and 10 μm.

Finally, in the following, we would like to address the issue of material selection for making the reflector. There are quite a lot of choices for grating, substrate, and low-refractive-index material in between as long as they can provide the required optical property and are feasible for fabrication. We choose GaAs as the template because it is one of the most common substrates for making optoelectronic devices. Other substrates like InP or Si are also applicable, although the structure parameters need slight modification. The Ge layer can be replaced with any material having a high enough refractive index and being transparent in the desired wavelength range. The SiO_x is not the best selection for the low-refractive-index layer due to its strong absorption, as we have seen above. Because the absorption is due to the vibration modes of Si–O bonding, TiO_2, for example, could be used instead to avoid it. Other dielectric material with low refractive index could be used, if available.

4. Conclusion

We have presented the design and fabrication of a new long-wavelength mid-IR mirror using the GMR effect. The high reflectivity (>95%) at 8 μm has been obtained with a total film thickness of about 2 μm. Although the high-reflection bandwidth is depressed by the strong absorption of the SiO_x layer, our design is feasible and easy for further integration with other mid-IR optical devices. One immediate application is fabricating a resonant cavity-enhanced quantum-dot IR photodetector by combining our reflector and the bottom DBR mirror reported in [22], which could significantly enhance its external quantum efficiency so its operating temperature could be increased.

This work was financially supported by NSC and by the ATU Program of MOE in Taiwan. We thank the Center of Nano Science and Technology at NCTU for their equipment support.

References

1. A. V. Barve, S. J. Lee, S. K. Noh, and S. Krishna, "Review of current progress in quantum dot infrared photodetectors," Laser Photon. Rev. **4**, 738–750 (2010).
2. Y. Yao, A. J. Hoffman, and C. F. Gmachl, "Mid-infrared quantum cascade lasers," Nat. Photonics **6**, 432–439 (2012).
3. G. A. Golubenko, A. S. Svakhin, V. A. Sychugov, and A. V. Tishchenko, "Total reflection of light from a corrugated surface of a dielectric waveguide," Sov. J. Quantum Electron. **15**, 886–887 (1985).
4. R. Magnusson and S. S. Wang, "New principle for optical filters," Appl. Phys. Lett. **61**, 1022–1024 (1992).
5. S. Peng and G. M. Morris, "Resonant scattering from two-dimensional gratings," J. Opt. Soc. Am. A **13**, 993–1005 (1996).
6. S. Peng and G. M. Morris, "Experimental demonstration of resonant anomalies in diffraction from two-dimensional gratings," Opt. Lett. **21**, 549–551 (1996).
7. Y. Zhou, M. C. Y. Huang, C. Chase, V. Karagodsky, M. Moewe, B. Pesala, F. G. Sedgwick, and C. J. Chang-Hasnain, "High-index-contrast grating (HCG) and its applications in optoelectronic devices," IEEE J. Sel. Top. Quantum Electron. **15**, 1485–1499 (2009).
8. C. F. R. Mateus, M. C. Y. Huang, Y. Deng, A. R. Neureuther, and C. J. Chang-Hasnain, "Ultrabroadband mirror using low-index cladded subwavelength grating," IEEE Photon. Technol. Lett. **16**, 518–520 (2004).
9. S. S. Wang, R. Magnusson, J. S. Bagby, and M. G. Moharam, "Guided-mode resonances in planar dielectric layer diffraction gratings," J. Opt. Soc. Am. A **7**, 1470–1474 (1990).
10. A. Sharon, D. Rosenblatt, and A. A. Friesem, "Resonant grating-waveguide structures for visible and near-infrared radiation," J. Opt. Soc. Am. A **14**, 2985–2993 (1997).
11. K. W. Lai, Y. S. Lee, Y. J. Fu, and S. D. Lin, "Selecting detection wavelength of resonant cavity-enhanced photodetectors by guided-mode resonance reflectors," Opt. Express **20**, 3572–3579 (2012).
12. V. Karagodsky, C. Chase, and C. J. Chang-Hasnain, "Matrix Fabry-Perot resonance mechanism in high-contrast gratings," Opt. Lett. **36**, 1704–1706 (2011).
13. L. C. Botten, T. P. White, A. A. Asatryan, T. N. Langtry, C. M. de Sterke, and R. C. McPhedran, "Bloch mode scattering matrix methods for modeling extended photonic crystal structures. I. Theory," Phys. Rev. E **70**, 056606 (2004).
14. H. S. Ling, S. Y. Wang, C. P. Lee, and M. C. Lo, "Long-wavelength quantum-dot infrared photodetectors with operating temperature over 200 K," IEEE Photon. Technol. Lett. **21**, 118–120 (2009).
15. C. C. Wang and S. D. Lin, "Resonant cavity-enhanced quantum-dot infrared photodetector with sub-wavelength grating mirror," J. Appl. Phys. **113**, 213108 (2013).
16. O. Parriaux, T. Kaempfe, F. Garet, and J. L. Coutaz, "Narrow band, large angular width resonant reflection from a periodic high index grid at terahertz frequency," Opt. Express **20**, 28070–28081 (2012).
17. I. R. Srimathi, M. K. Poutous, A. J. Pung, Y. Li, R. H. Woodward, E. G. Johnson, and R. Magnusson, "Mid-infrared guided-mode resonance reflectors for applications in high power laser systems," in *IEEE International Photonics Conference (IPC)* (2012), pp. 822–823.
18. M. G. Moharam and T. K. Gaylord, "Rigorous coupled-wave analysis of planar grating diffraction," J. Opt. Soc. Am. **71**, 811–818 (1981).
19. RSoft Design Group's website for DiffractionMOD simulation tool, http://www.rsoftdesign.com/products.php?sub=Component+Design&itm=DiffractMOD.
20. N. Yamamoto and S. Noda, "Fabrication and optical properties of one period of a three-dimensional photonic crystal operating in the 5–10 μm wavelength region," Jpn. J. Appl. Phys. **38**, 1282–1285 (1999).
21. C. K. Wong, H. Wong, C. W. Kok, and M. Chan, "Silicon oxynitride prepared by chemical deposition as optical waveguide materials," J. Cryst. Growth **288**, 171–175 (2006).
22. T. Asano, C. Hu, Y. Zhang, M. Liu, J. C. Campbell, and A. Madhukar, "Design consideration and demonstration of resonant-cavity-enhanced quantum dot infrared photodetector in mid-infrared wavelength regime (3–5 μm)," IEEE J. Quantum Electron. **46**, 1484–1491 (2010).